Preparation of High Water-absorbing Hydrogel Based on Grafted Micro/Nano Cellulose

Suri Gala,[a,b,1] Yi Mao,[a,b,1] Xiuchun Bao,[a,b] Bing Ma,[a,b] Yanfei Pan,[a,b] and Jintian Huang [a,b,]*

An absorbent hydrogel with high-permeable solution resistance was prepared by free radical polymerization and crosslinking, by the process of micro/nano cellulose grafting with acrylic acid (AA) and 2-acrylamide-2-methyl propyl sulfonic acid (AMPS). Imbibition swelling curves revealed that absorbency of the hydrogel reached 70.2, 483.9, and 436.7 g/g in 0.9 wt% sodium chloride solution, 3 wt% urea solution, and rainwater, respectively. Fourier transform infrared results confirmed that acrylic acid (AA) and 2-acrylamide-2-methyl propyl sulfonic acid (AMPS) were grafted onto the micro/nano cellulose surface and the fiber structure persisted. Analysis with a confocal laser scanning microscope showed many pores on the polymer's surface. Roughness became larger after grafting, which was conducive to water absorption capacity. Scanning electron microscopy (SEM) results showed that the main morphology of micro/nano cellulose did not change. BET results showed the presence of mesopores and macropores, which made the absorbent hydrogel highly permeable, allowing the internal and external absorbent groups to absorb water. H NMR confirmed that the cellulose was grafted with water-absorbent groups. In addition, lamellar structure and porous network morphology showed graft reaction occurred on the surface of micro/nano cellulose. The hydrogel has potential for agriculture and forestry, including in desertified and self-irrigated areas.

Keywords: Absorbent hydrogel; Micro/nano cellulose; Graft copolymerization; High-permeable solution resistance

*Contact information: a: College of Material Science and Art Design, Inner Mongolia Agricultural University, Hohhot, China 010018; b: Inner Mongolia Key Laboratory for Sand Shrubs Fibrosis and Energy Development and Utilization, Hohhot, China 010018; 1: These authors contributed equally to this work; *Corresponding author:jintian_h@163.com*

INTRODUCTION

Drought has a huge impact on agriculture and therefore causes economic losses (Wu *et al.* 2020). The addition of a water-retaining agent can effectively restrain the rapid water loss of soil (Liu *et al.* 2020). In an absorbent hydrogel (hydrogel), long-chain molecules containing many strongly water-absorbing groups are crosslinked with each other to form a three-dimensional network structure (Hubbe *et al.* 2013). The absorbed water is not easily extruded under pressure on account of the restriction on water molecules movement. An absorbent hydrogel not only has excellent water absorption, but also relatively stable water retention (Lan *et al.* 2019). Absorbent hydrogels are widely used, especially in physiological health, food processing, drug transmission (Dai *et al.* 2014), wastewater treatment (Abdelwahab *et al.* 2015; Rahman *et al.* 2016), building materials (Song and He 2012), environmental protection, and functional materials (Kosinska *et al.* 2019).

When an absorbent hydrogel was used in agriculture, forestry irrigation, sewage treatment, petroleum exploitation, or as an aid to physical health, highly permeable performance was needed and need to achieve specified levels of performance (Quennouz *et al.* 2016). It is well known that polymers related to 2-acrylamido-2-methyl propane sulfonic acid (AMPS) have good salt resistance and thermal stability. Choi studied the kinetics of AMPS in aqueous solution (Choi *et al.* 2019). Absorbent hydrogels have achieved moderate levels of absorption of artificial blood and artificial urine (Awadallah and Mostafa 2014). Advances have been made in alleviating the loss of oil-field drilling well fluid and improving the thermal stability of dispersion capacity by the introduction of AMPS (Guo and Bu 2013). The adsorption of some toxic metal ions in aqueous solution and improvement of chemical stability has also been developed (Kumar *et al.* 2020). In addition, comprehensive ability of water absorbent hydrogel has been further studied by Mandal and Chakrabarty (2017).

In recent years, micro/nano cellulose, including microcrystalline cellulose (MCC) (Madrid and Abad 2015; Yang *et al.* 2017), nano crystalline cellulose (NCC) (Kabiri and Namazi 2014; Chauhan and Yan 2015), and bacterial nanocellulose (BNC) (Mohammadkazemi *et al.* 2015), have become widely used in new functional composites. There are numerous advantages of high strength, light weight, large specific surface area, biocompatibility, and biodegradability (Chen *et al.* 2017). Moreover, nanocrystalline cellulose has no use for pretreatment because the crystallinity is higher than that of natural cellulose; this means that a large proportion of the water-loving hydroxyl groups are enclosed in the crystalline zone and required to be dissolved in a specific solvent (Lu *et al.* 2017).

In this study, NCC is self-made and the experimental raw material is waste pulp. Undoubtedly, absorbent hydrogels using micro/nano cellulose as the backbone of graft polymerization have high tolerance for permeation of solutions and advantageous biodegradability compared to traditional absorbent hydrogels, most of which are produced on the basis of acrylic acid and acrylamide (Klemm *et al.* 2005). Hydrogels based on nanocellulose are likely to become a future direction in the development of water-absorbing material (Miao *et al.* 2012).

In many instances, for the sake of preparing some special properties of materials, priority is given to selected functional groups by chemical modification of cellulose (Habibi 2014) to expand its application field (Zaman *et al.* 2013). Considering the inadequate biodegradability of traditional absorbent hydrogel, grafting AA and AMPS onto micro/nano cellulose can advance high-permeable solution resistance and biodegradable properties (Saikia *et al.* 2012).

The intent of this work is to improve the permeability of absorbent hydrogel, which is environmentally friendly, to expand its application to the irrigation of agriculture and forestry in arid regions. This was achieved by the graft copolymerization of AA and AMPS onto micro/nano cellulose through free radical polymerization (Varaprasad *et al.* 2017). The morphological characteristics and water absorption properties of the products were characterized by means of absorbency test, Fourier transform infrared (FTIR) spectroscopy, confocal laser scanning microscopy, and scanning electron microscopy analysis. Optimum conditions for preparation of absorbent hydrogel were also found.

EXPERIMENTAL

Materials

Micro/nano cellulose, 100 to 500 nm in diameter, were supplied from Hangzhou Han Technology Co., Ltd. (Hangzhou, China). Acrylic acid (analytical purity) was purchased from Shanghai Macklin Biochemical Co., Ltd. (Shanghai, China). The 2-acrylamido-2-methyl propane sulfonic acid (98%) was purchased from Alfa Aesar (China) Chemicals Co., Ltd. (Shanghai, China). Ammonium peroxydisulfate (APS) as initiator and N,N'-methylene diacrylamide (MBA) as a crosslinking agent were obtained from Tianjin North Union Fine Chemicals Development Co., Ltd. (Tianjin, China), and Shandong West Asia Chemical Industry Co., Ltd. (Shandong, China), respectively. The other chemical reagents were of analytical grade, and all solutions were prepared with deionized water.

Synthesis of AA/AMPS-Micro/Nano Cellulose Composite Absorbent Hydrogel

Preliminary preparation of graft polymerization

The micro/nano cellulose was adjusted between 1 and 2% in solid content and treated by ultrasonic treatment for 20 min, which changed from agglomerated state to a dispersed state. Quantitative AMPS was dissolved in 5 mL of deionized water. A 25% sodium hydroxide solution was injected when the neutralization of AMPS solution reached 70%. Additionally, 25% sodium hydroxide solution was added dropwise into a small beaker filled with AA, which was put in ice water. The sodium hydroxide, AA, and ice water solution were dripped and stirred simultaneously, so that the heat dissipated adequately without the formation of floc deposition. The preparation method had the advantages of low cost, high efficiency, reaction conditions, reaction medium, safe operation and convenience for industrial production. The hygroscopicity and thermal stability of the hydrogel were improved. The amounts of substances mentioned above are noted in Table 1.

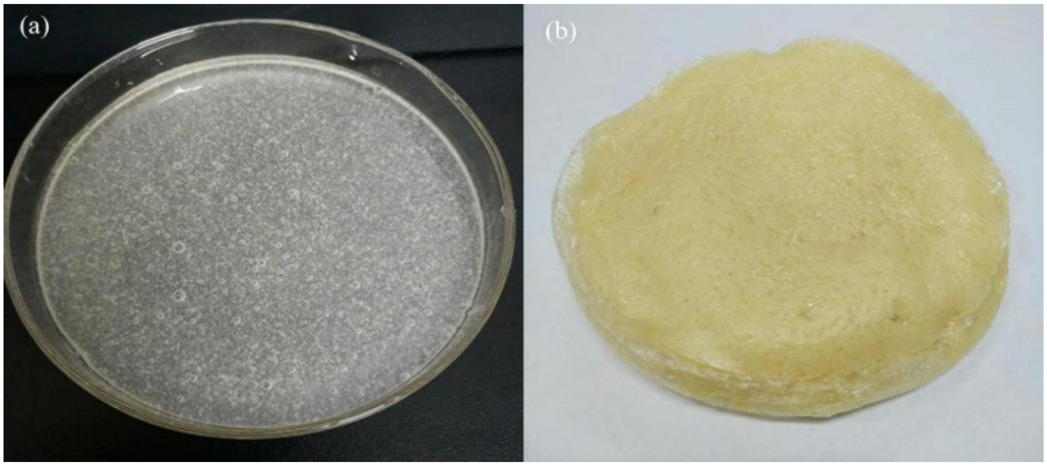

Fig. 1. (a) The hydrogel AR1 before drying and (b) the hydrogel AR2 after drying

Graft polymerization by free radical polymerization

The preparation of absorbent hydrogel was performed according to a typical binary graft polymerization process. The initiator was first decomposed to produce primary free radicals, which generated free radicals on micro/nano cellulose chain and acrylic acid monomers. This brought about chain reaction polymerization between micro/nano cellulose and acrylic acid monomer. Meanwhile, the crosslinking agent reacted between the generated branch chains and connected them into a network structure. The experimental scheme was designed according to influencing factors using a single factor method, as shown in Table 1. The 14 mL treated micro/nano cellulose was added to a three-neck flask that was equipped with an agitating device fixed in a water bath at constant temperature. Afterwards, nitrogen was let into the flask for 10 min to remove oxygen. The APS, which was dissolved in 2 mL distilled water, was injected into the flask to initiate the reaction, and form the primary free radical. Ten minutes later, two kinds of neutralizing solutions (Table 1) were poured into the flask, stirred, and mixed at a speed of 150 rpm. Polymerization was conducted by an addition reaction between micro/nano cellulose and two anionic hydrophilic monomers to form monomer free radicals. The inlet of nitrogen was ceased after 10 min. The MBA was added into distilled water to give a final concentration of 0.8 g/mL. When the mixed system changed thickness, quantitative MBA solution was injected to start the crosslinking reaction, until a bulky gel named as absorbent hydrogel AR1 (Fig. 1a) was obtained. Finally, AR1 was placed in the concave silica gel and dried for 40 min at 140 °C to obtain the ultimate composite absorbent hydrogel AR2 (Fig. 1b). The uncharted amount of substances and the temperature set mentioned above are listed in Table 1.

Table 1. Design of Single Factor Experiment

M (APS) / M_A	M (MBA) / M_A[a]	Temp. (°C)	Neutralization Degree	M(AA) / M (AMPS)
1.5:9	0.3:9	55	75	6:3
2:9	0.3:9	55	75	6:3
2.5:9	0.3:9	55	75	6:3
3:9	0.3:9	55	75	6:3
3.5:9	0.3:9	55	75	6:3
3:9	0.2:9	55	75	6:3
3:9	0.25:9	55	75	6:3
3:9	0.3:9	55	75	6:3
3:9	0.35:9	55	75	6:3
3:9	0.4:9	55	75	6:3
3:9	0.3:9	45	75	6:3
3:9	0.3:9	50	75	6:3
3:9	0.3:9	55	75	6:3
3:9	0.3:9	60	75	6:3
3:9	0.3:9	65	75	6:3
3:9	0.3:9	60	60	6:3
3:9	0.3:9	60	65	6:3
3:9	0.3:9	60	70	6:3
3:9	0.3:9	60	75	6:3
3:9	0.3:9	60	80	6:3
3:9	0.3:9	60	75	9:0
3:9	0.3:9	60	75	8:1
3:9	0.3:9	60	75	7:2
3:9	0.3:9	60	75	6:3
3:9	0.3:9	60	75	5:4

[a] M_A: the gross mass of AA and AMPS

Measurement of water absorption in different liquid

The completely dry AR2 was shattered in a universal grinder and separated by an 80-mesh sieve. The AR2 of different mesh were bagged and marked.

Approximately1 g of granular hydrogel from each single factor group (Table 1) was placed into sufficient rainwater, 0.9 wt% sodium chloride solution, and 3 wt% urea solution at room temperature for 30 min to reach the swelling equilibrium. The unabsorbed water was strained off with a 200-nylon mesh sieve bag. Finally, the water absorption of the absorbent hydrogel was calculated with the Eq. 1,

$$\text{Swelling (g/g)} = (m_1 - m_0) / m_0 \tag{1}$$

where m_0 (g) and m_1 (g) are the weights of hydrogel absorbed water before and after adsorption saturation, respectively.

Methods

FTIR spectroscopy

The sample was compressed by potassium bromide (KBr) with a litter hydrogel powder. The FTIR spectra were obtained by using a TENSORTM Type27 series FTIR spectrometer from Bruker Corporation (Beijing, China), that scanned in the wavelength range of 4000 to 400 cm^{-1}.yh

Confocal laser scanning microscope (CLSM)

The fully dried absorbent hydrogel AR2 was observed by a VK-X series laser microscope system (Keyence, Ōsaka, Japan) for shape measurement with a red diode laser wavelength of 658 nm and resolution of 5 nm. The surface scanning and imaging of the sample were performed to observe and analyze the three-dimensional structure without damage.

Scanning electron microscopy

The morphology of the grafted polymer was observed by a scanning electron microscope (SEM) produced by Hitachi S-4800 (Hitachi, Tokyo, Japan).

H-Nuclear magnetic resonance (H NMR)

Nuclear magnetic resonance analyses were conducted using a Brouck 600MHz AVANCE III instrument (Brooke Beurspine, Shanghai, China). Using a 5 mm PABBO probe, the test frequency was 600 MHZ, pulse 12.95 microseconds, and the number of scans 128.

TG Analysis

The powder hydrogel was evenly spread in the Pt crucible and put into the sample support. NETZSCH STA 409 PC synchronous thermal analyzer was used (NETZSCH-Gerätebau GmbH, Selb, Germany). Under the nitrogen flow protection with a flow velocity of 10 °C/min, the samples were tested by TGA, and the temperature range was set as 0 to 800 °C.

Nitrogen adsorption-desorption measurement

The pore structures of samples were characterized by a N_2 adsorption technique at 77 K using Micromeritics (Beishide Instrument technology, Beijing, China). Specific surface areas were analyzed by the Brunauer-Emmett-Teller (BET) model and the BET specific surface areas was calculated by Eq. 1. The pore size distribution was presented by the Barrett-Johner-Halenda (BJH) model,

$$A_s = \frac{\mathrm{V}_\mathrm{m} \times N \times a_m}{22400 \times W} \times 10^{-18} \tag{1}$$

where A_s is the specific surface area of the sample to be tested (m_2/g), V_m is the saturated adsorption capacity of a single layer of nitrogen under standard conditions (mL), a_m is the equivalent maximum cross-sectional area of the nitrogen molecule, with a value of 0.162 nm, W is the quality of the tested sample (g), and N is Avogadro's constant, with a value of 6.02 x 10^{23}.

RESULTS AND DISCUSSION

Influence of Micro/nano Cellulose Dosage on Polymerization Reaction

It can be seen in Fig. 2 that when other reaction conditions are fixed, the amount of cellulose increased with the range of 7% and 15%. The absorbency of 0.9 wt% brine, 3 wt% urea solution, and rainwater could reach up to 62.9, 395.5, and 370.1 g/g, respectively. The most significant effect was when the cellulose content accounted for 11% of the hydrogel.

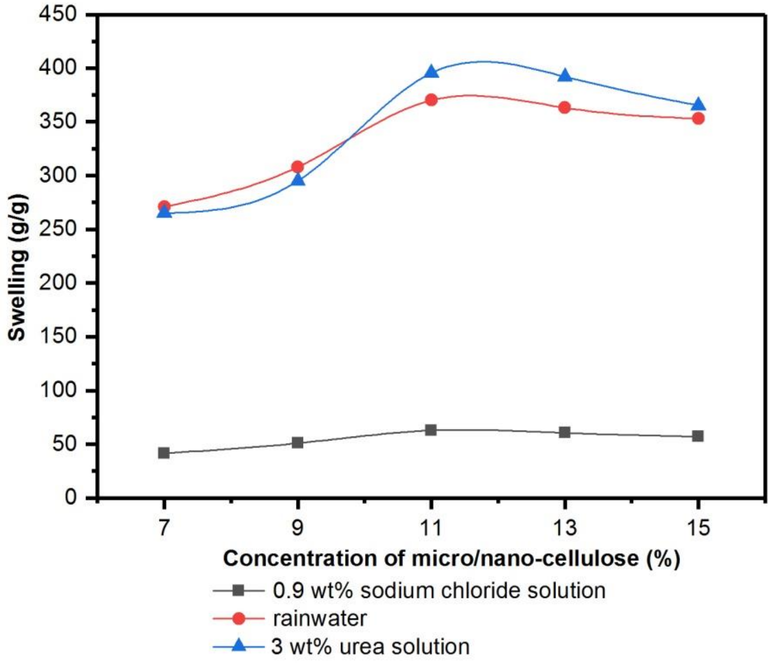

Fig. 2. Swelling of different liquids at five different micro/nano cellulose mass, under the following reaction conditions: 70% neutralized AA, 2.5% initiator and 0.25% crosslinking agent at 55 °C

The dependency of the liquid absorption curve trend on the amount of micro/nano cellulose was mainly attributable to changing the amount of hydrophilic groups. With the increase of dosage of cellulose, the number of hydrophilic groups, such as sulfonic group, carboxyl, amino, hydroxyl content increase sharp, leading to increase of the number of the main chain of the cellulose, decreases of the apparent crosslinking density, and improvement of hydrophilicity. However, when the amount of cellulose dosage exceeded 11%, the cellulose molecules tended to agglomerate, resulting in non-uniform reaction between monomers, and the homopolymer reaction between monomers and then generating a large number of small molecular polymers, which reduced the absorbency. The optimal process in this study contained a large amount of cellulose, which is beneficial for environmental protection.

Influence of Initiator (APS) Dosage on Polymerization Reaction

It is clear that absorbency curves all showed a trend of decrement after the first increment with increased amount of initiator (Fig. 3). The electrolyte uptake reached the maximum value when the amount of initiator was 3%. Maximum absorbency of 0.9 wt% sodium chloride solution, 3 wt% urea solution, and rainwater were 48.2, 215.4, and 239.7 g/g, respectively. The effect of initiator dosage on absorbency was mainly achieved by changing the length of molecular chain in the hydrogel. The formation of free radicals on micro/nano cellulose were less effective, which led to failure to effectively forma three-dimensional macromolecular network when the amount of initiator was too low (Klinpituksa and Kosaiyakanon 2017). Nevertheless, the speed of cessation of reaction was accelerated when the amount of initiator was too large, which made the active center too late to terminate polymerization. The self-polymerization of AA was initiated to produce low molecular weight polymers and amplify crosslinking density, which reduced the liquid absorption capacity of the hydrogel (He *et al.* 2017).

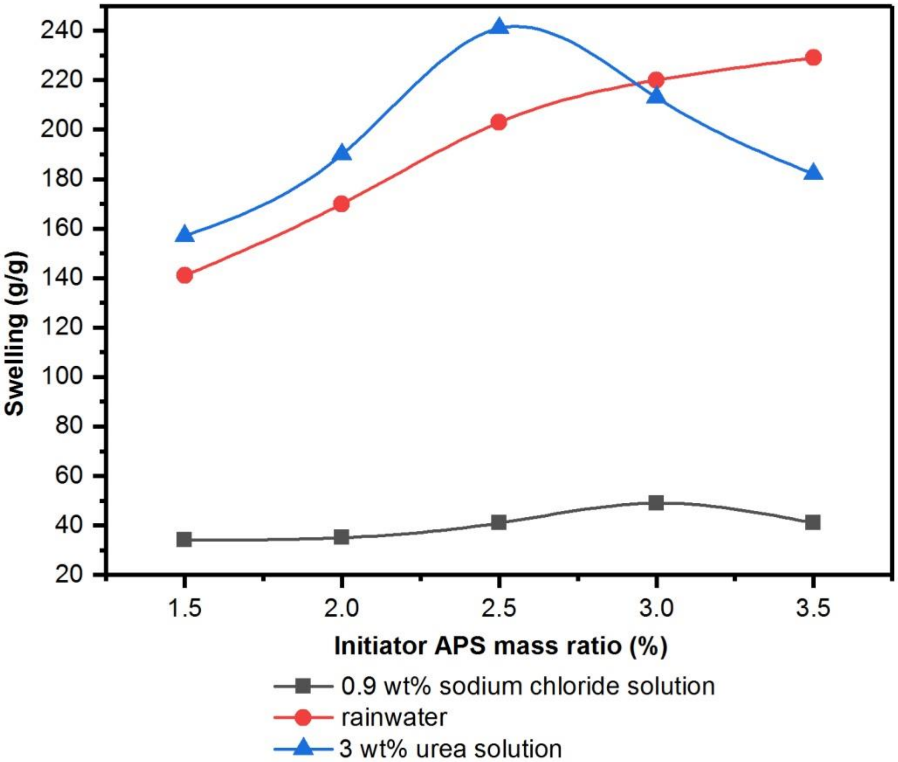

Fig. 3. Swelling of different liquids at five different initiator (APS) mass ratios, under the following reaction conditions: 11% micro/nano cellulose, 70% neutralized AA, and 0.25% crosslinking agent at 55 °C

Influence of Crosslinking Agent (MBA) Dosage on Polymerization Reaction

The curve of absorbency increased first and decreased then with increased amount of crosslinking agent (Fig. 4). There were still many macromolecular chains in the hydrogel without crosslinking, which indicated there was soluble component. This made the hydrogel soluble in water when the amount of crosslinking agent was too low. The peak value appeared at 0.3% of crosslinking agent addition, which can be ascribed to the large network of pores that made water molecules easy to penetrate the network structure of composite materials. Maximum absorbency of 0.9 wt% sodium chloride solution, 3 wt% urea solution, and rainwater were 51.7, 293.4, and 282.6 g/g, respectively. However, the absorbency was abated when too much crosslinking agent was used. The key reasons were as follows: the crosslink density of the hydrogel was too large, the molecular chain between the crosslinking points became shorter, the network structure of the hydrogel was difficult to stretch, and the elastic strength was reduced (Hua and Wang 2009).

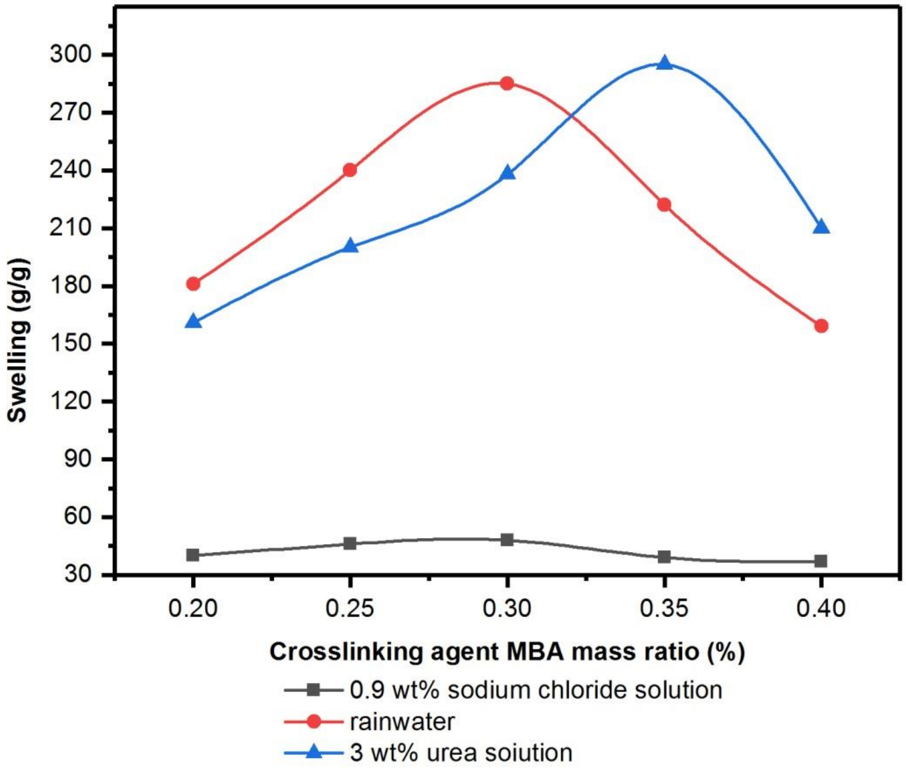

Fig. 4. Swelling of different liquids at five different crosslinking agent (MBA) ratios, under the following reaction conditions: 11% micro/nano cellulose, m(AA):m(AMPS) 6:3, 70% neutralized AA, and 3% initiator (APS) at 55 °C

Influence of Reaction Temperature on Polymerization Reaction

Activation energy is required for the free radical initiator reaction, and it can only be achieved above a certain temperature level. The water absorbency increased with the rise of reaction temperature (Fig. 5). Maximum absorbency of 0.9 wt% sodium chloride solution, 3 wt% urea solution, and rainwater were 57.1, 365.4, and 350.8 g/g, respectively. Additionally, initiator induction time was shortened, the monomer conversion rate was increased, and hydrogel crosslinking degree became larger. Thus, the three-dimensional network structure formed gradually (Wu *et al.* 2012). When the temperature was higher than 60 °C, the self-assembly reaction between monomers was extremely easy to induce, chain transfer and chain termination rate were expedited, and hydrophilic groups on the main chain were reduced. The above-mentioned phenomenon made further efforts to decrease the hydrogel absorption capacity (Liu *et al.* 2008).

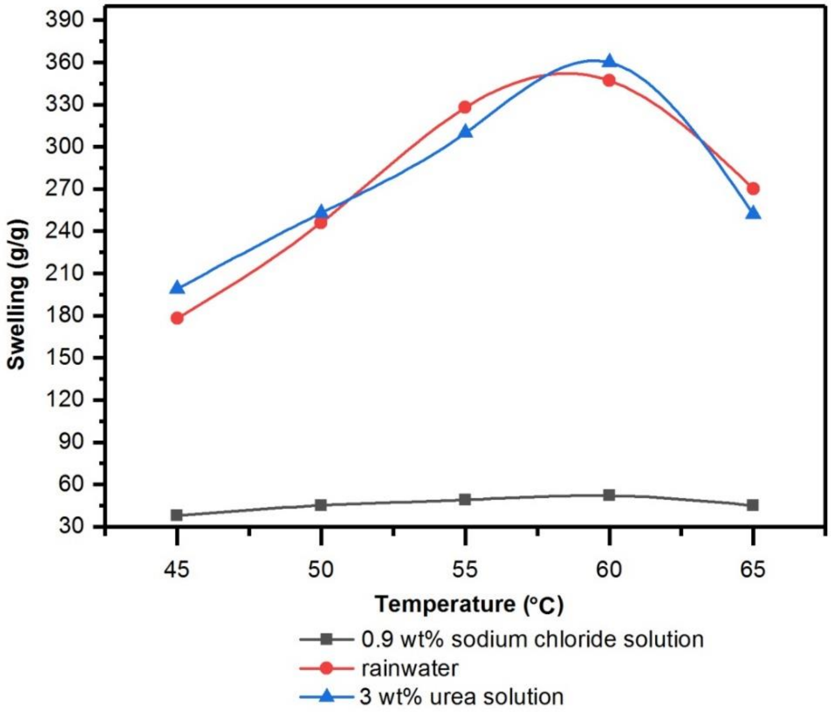

Fig. 5. Swelling of different liquid at five different temperatures, under the following reaction conditions: 11% micro/nano cellulose, m(AA):m(AMPS) 6:3, 70% neutralized AA, 3% initiator, and 0.3% crosslinking agent

Influence of AA Neutralization Degree on Polymerization Reaction

The absorbing mechanism is determined by sodium carboxylate groups (-COONa) ionized in aqueous solution, which engenders electrostatic repulsion. The higher concentration of sodium (Na^+) inside makes the internal and external solutions of hydrogel form osmotic pressure, which allows water to enter hydrogel and to increase the capacity of water adsorption. The absorbency curves first increased and then decreased with the increase of AA neutralization degree. The peak value was reached when the AA neutralization degree was 75%. Maximum absorbency of 0.9 wt% sodium chloride solution, 3 wt% urea solution, and rainwater were 64.9, 332.4, and 366.2 g/g, respectively. When the degree of polymerization was too low, the reaction of AA monomer was large with fast polymerization speed and short graft chain generation. Simultaneously, the content of sodium carboxylate (-COONa) in hydrogel molecules was less, which made the concentration of $-COO^-$ and Na^+ ions produced by -COONA ionization limited when absorbing. The result was that osmotic pressure decreased. Moreover, the repulsive force between the same ions was weakened and the extension of the network structure was affected. However, when the neutralization degree of AA was over 75%, the alkaline concentration was too high, and the activity of ions was low. The synergistic effect of carboxylic acid sodium and amide group was weakened, which suppressed the water storage capacity of the three-dimensional network (Wu and Liu 2007).

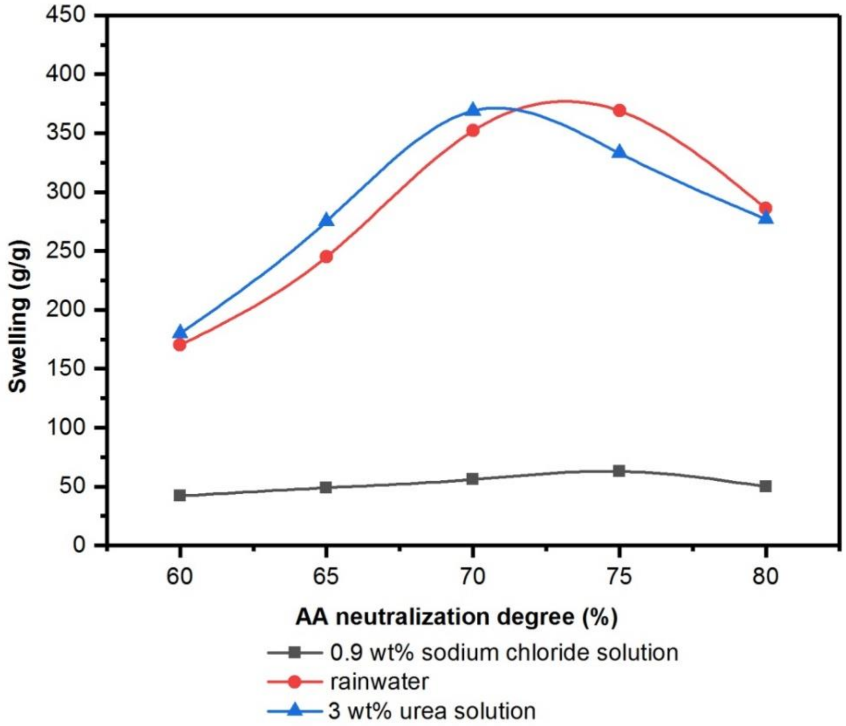

Fig. 6. Swelling of different liquids at five different AA neutralization degree percentages, under the following reaction conditions: 11% micro/nano cellulose, m(AA):m(AMPS) 6:3, 3% initiator, and 0.3% crosslinking agent at 60 °C

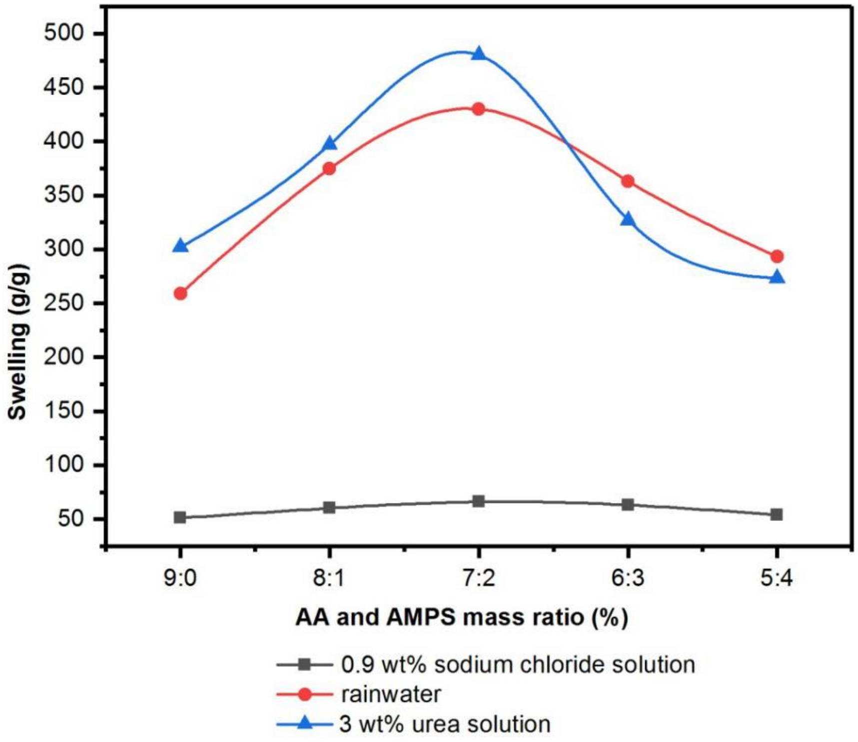

Fig. 7. Swelling of different liquids at five different mass ratios of AA and AMPS, under the following reaction conditions: 11% micro/nano cellulose, 75% neutralized AA, 3% initiator, and 0.3% crosslinking agent at 60 °C

Influence of m(AA):m(AMPS) on Polymerization Reaction

From Fig. 7, beginning with the increase of AMPS dosage, the number of anionic (COO$^-$) in the polymer network increased, and the degree of ionization of water was promoted. The pulsive electrostatic ion increased, so the osmotic pressure of network inside and outside was enhanced, with the absorbency of hydrogel increasing (Liu *et al.* 2009). The crosslinking degree of the polymer was directly affected with the decrease of AA dosage, which increased soluble fraction of the hydrogel and decreased the water absorption (Chen *et al.* 2005). When m(AA):m(AMPS) was 7:2, maximum absorbency of 0.9 wt% sodium chloride solution, 3 wt% urea solution, and rainwater were 70.2, 483.9, and 436.7 g/g, respectively.

FTIR Analysis

For the curve of micro/nano cellulose (Fig. 8(a)), the peaks at 3443, 2894, 1421, and 1066 cm^{-1} correspond to the hydroxyl stretching vibration peak (-OH) caused by hydrogen bonding, the peak of methylene stretching vibration (C-H), the stretching vibration peak caused by C-H variable angle, and the beta-(1,4) glycosidic bond in the fingerprint region, respectively (Fig. 8). These are representative of the micro/nano cellulose characteristic absorption peaks (Ma *et al.* 2011).

The curve of AA/AMPS-g-micro/nano cellulose composite absorbent hydrogel (Fig. 8 (b)) shows new characteristic absorption peaks compared to curve (Fig. 8 (a)). The stretching vibrational absorption peaks of C=O and N-H that belong to amide II and amide I arose at 1666 and 1572 cm^{-1}, respectively. (Wen *et al.* 2017). The C-N stretching vibration peak appeared at 1410 cm^{-1}, which pertains to the amide group. Otherwise, the antisymmetric and symmetric stretching vibrational absorption peaks of sulfonate group (S=O) appeared at 1221 and 1046 cm^{-1}, which is part of the AMPS structure (Saikia *et al.* 2012). The peaks at 1721 and 1455 cm^{-1}are from stretching vibration absorption of -COOH and -COO$^-$. These demonstrated that AMPS and AA have been grafted on to the micro/nano cellulose macromolecular skeleton.

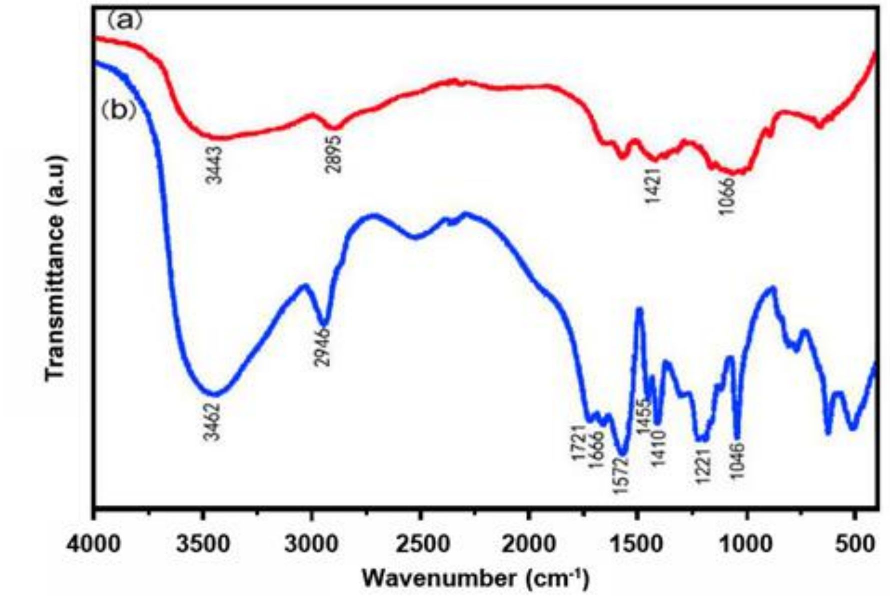

Fig. 8. FTIR spectra of micro/nano cellulose (a) and AA/AMPS-g-micro/nano cellulose composite absorbent hydrogel (b)

Confocal Laser Scanning Microscope (CLSM) Analysis

As shown in Fig. 9, threshold detection was implemented based on the height of the reflected laser profile. Figure 9(a) is the confocal laser image of a region on its surface, which displays various sized pores of the grafted polymer surface. Figure 9(b) reflects the cross-section and roughness of the surface, one-third of the top edge in Fig. 9(a). Partial parameters were obtained from testing: R_a was 40 μm, S_a was 276 μm. The surface of the grafted polymer was rugged from pore depth and roughness due to the existence of pores. Figure 9(c) and (d) reflect the degree of concave- convex polymer surface bumps.

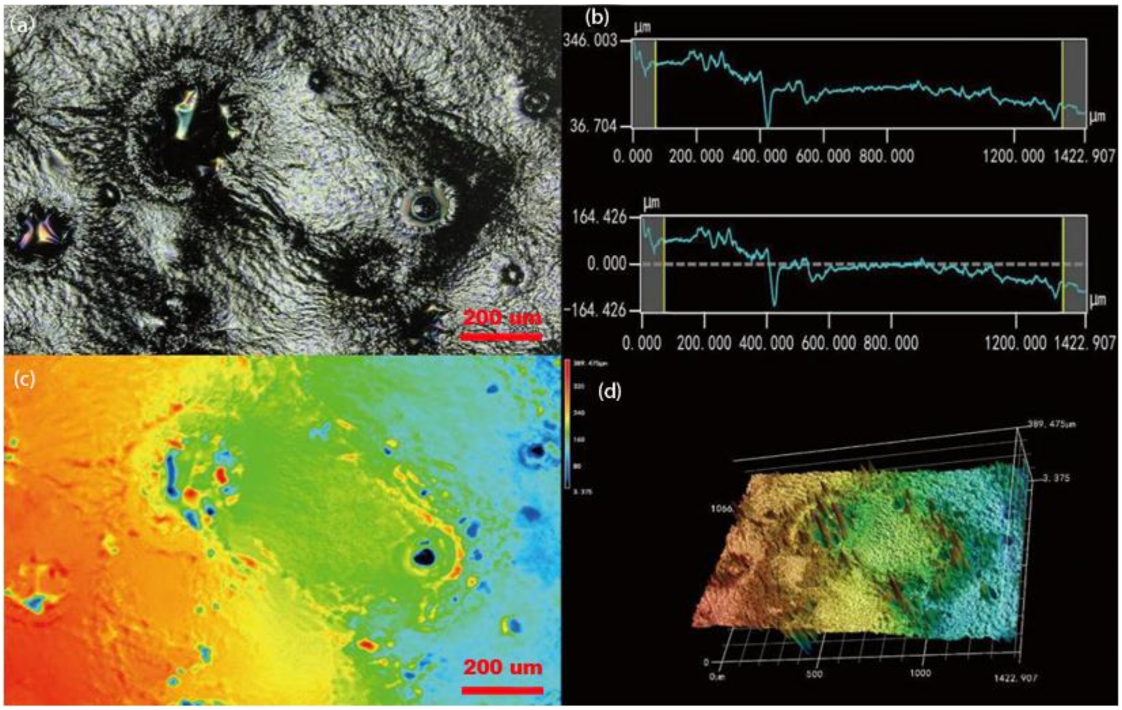

Fig. 9. (a): 16-bit color laser confocal image; (b): contour graph image; (c): image of relative superiority or inferiority; (d): 3D color image of hydrogel AR2 surface with magnification in 200 μm

TG Analysis

It was seen that the main thermal decomposition process was divided into three stages, as shown in Fig. 10. The first thermal decomposition stage of the absorbent hydrogel occurred within the temperature range from 38 to 299 °C. The initial decomposition temperature increased, and the weight loss rate increased to 11.3%. The moisture volatilization in this stage reduced the amount of crystalline water inside the hydrogel. Second stage occurred between 300 and 394 °C. Thermal decomposition temperature increased and the rate of weight loss was reduced from 61.6% to 15.9% compared with cellulose. The monomer reacted, and a small molecule weight compounds were generated at lower amounts in the process of the absorbent hydrogel synthesis. The formation of the polymer network structure made the hydrogel system dense and orderly, which improved internal thermal stability. The third stage temperature occurred ranging from 395 to 544 °C. The maximum decomposition temperature was 431 °C, compared to the cellulose decomposition temperature 341 °C, further illustrating that the ternary grafted product had good thermal stability, and this one phase of the rate of weight loss increased from 10.53% to 23.6%. It may be that most of the hydrophilic group turned into free, and decreased internal binding force and crystallinity, leading to thermal stability.

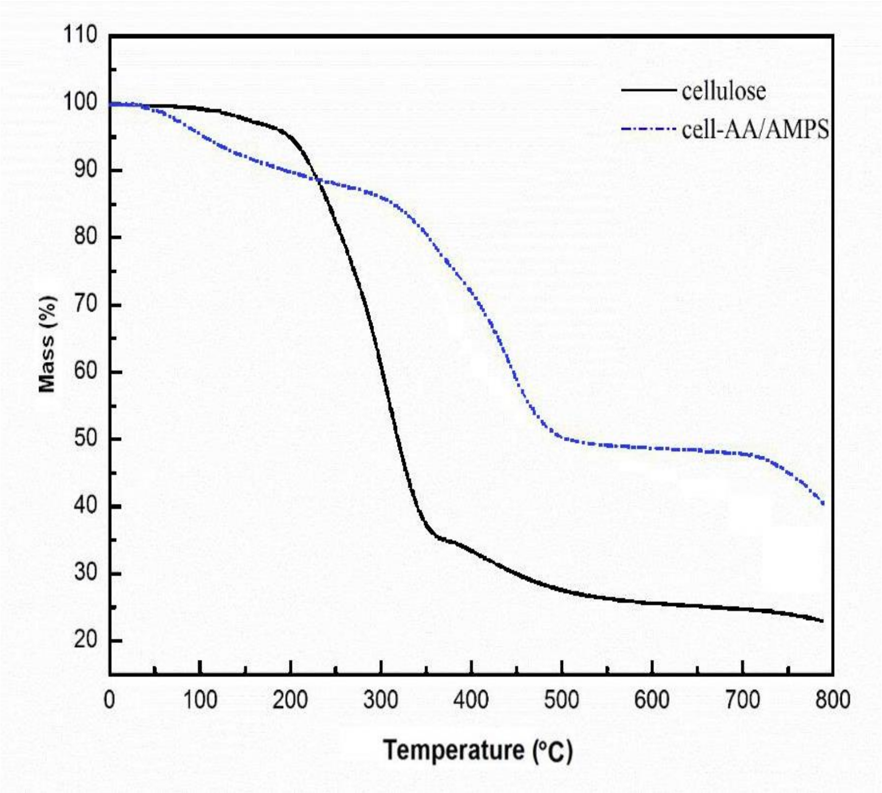

Fig. 10. TG of micro/nano cellulose and absorbent hydrogel after ternary grafting

SEM Analysis

Figure 11(a) is a SEM image of grafted polymer at 5,000 times magnification. It shows that the surface of the polymer presents lamellar and schistose distributions. Figure 11(b), (c), and (d) are scanning electron microscope images observed from different angles at 50,000 times magnification. It is apparent from Fig. 11(b) that there were many holes with different sizes on the surface of the polymer, with cracks and voids, which make the hydrogel possess superior surface area and pore volume. The ability of absorbency was also improved (Wang *et al.* 2010). An emblematical crosslinked type image is shown in Fig. 11(c), which can be perceived in the form of adhesion like rupture after crosslinking. The structure of the fiber is clearly visible with sodium acrylate and sodium sulfonate filling in the fibers and acting as part of the network (Chen and Parl 2000). The structure in Fig. 11(d) is like the porous gel network formed by crosslinking, which form capillary channels and enhance the swelling properties of the gel (Qiao *et al.* 2016).

Figure 12 and Table 2 showed the composition of micro/nano cellulose and absorbent hydrogel elements. It can be seen that the content of C and O elements in micro-nano cellulose were 46.8% and 53.2%, respectively. The content of C, O, Na, S and N elements in the absorbent hydrogel were 43.5%, 45.67%, 5.35%, 3.81% and 1.67%, respectively.

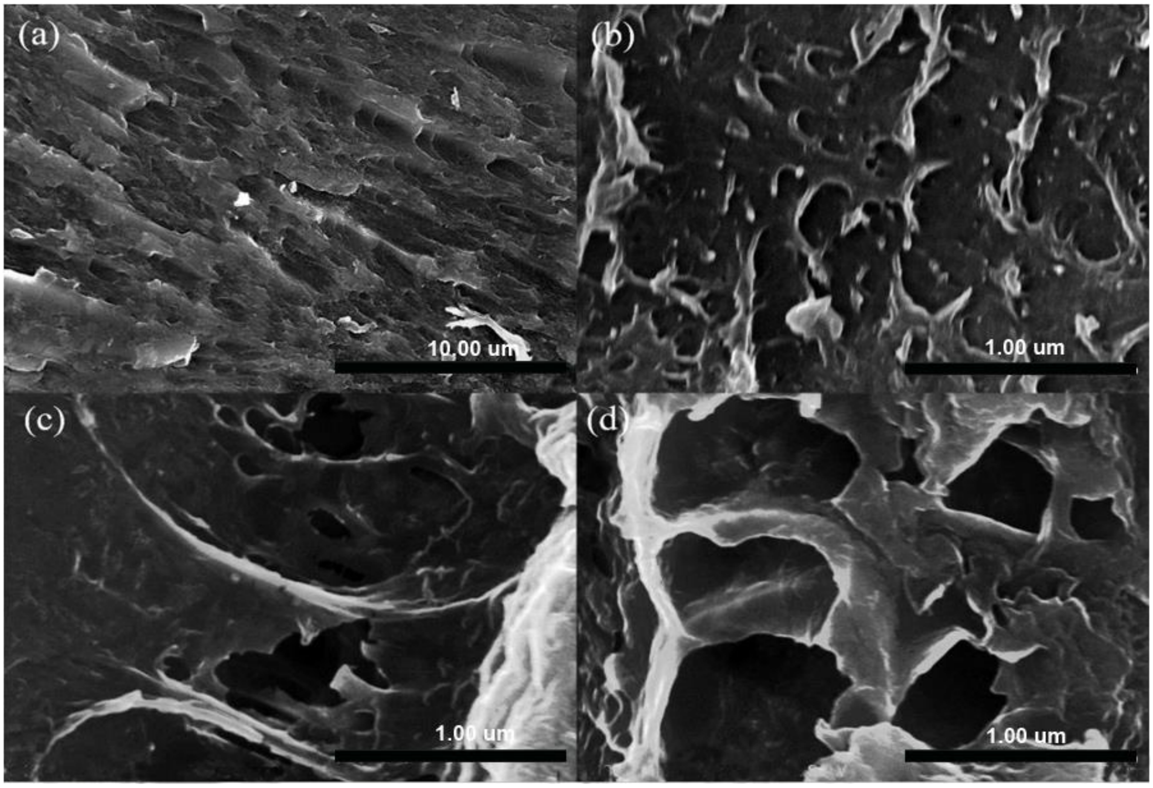

Fig. 11. SEM micrograph of absorbent hydrogel prepared under the optimum conditions

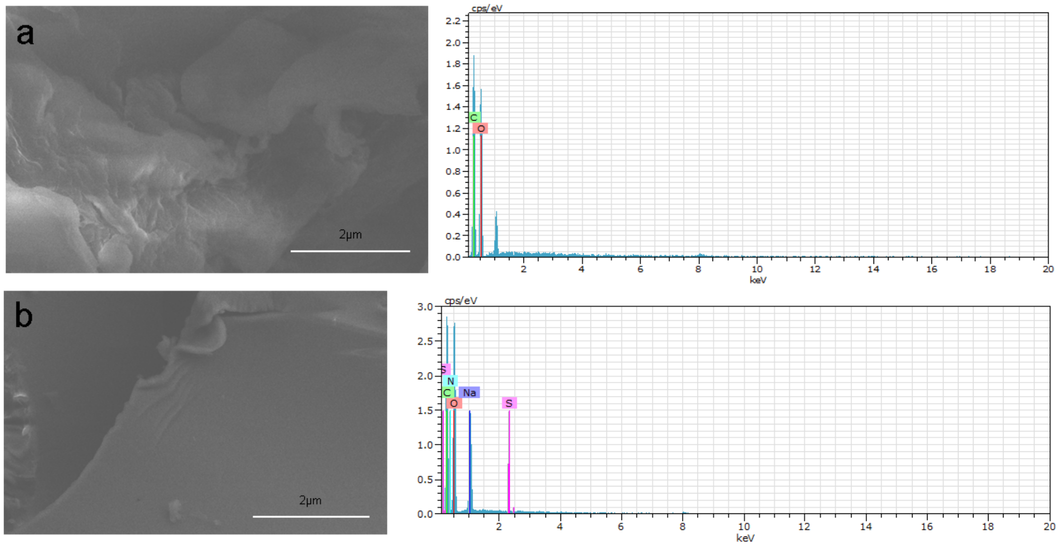

Fig. 12. The elements composition of micro/nano cellulose (a) and absorbent hydrogel (b)

Table 2. Elemental Percentage Composition of Micro/nano Cellulose and Absorbent Hydrogel

Type	Elements composition (wt %)				
	C	O	Na	S	N
Micro/Nano Cellulose	46.84	53.16	0	0	0
Absorbing Hydrogel	43.5	45.67	5.35	3.81	1.67

BET Analysis

Nitrogen adsorption desorption experiment was carried out to elucidate the pore diameter distribution of the prepared absorbent hydrogel (Fig. 13 (a)). According to the classification of nitrogen adsorption-desorption isotherms by the International Union of Pure and Applied Chemistry (IUPAC), it can be known that the isotherms of nitrogen adsorption-desorption in Fig. 3a belong to type IV isotherms. In the region with low relative pressure, the adsorption capacity increases rapidly. In this stage, the adsorption of single molecular layer and the filling of micropores of super absorbent hydrogel are mainly completed. When the relative pressure is higher than 0.2, the adsorption capacity rises slowly, and the filling of mesopore is the main factor in this stage. When the relative pressure exceeds 0.8, the adsorption capacity increases rapidly again. In this stage, the adsorption is mainly carried out by macropores.

According to the BJH principle (formula 1), the nitrogen adsorption curve was calculated, and the mesoporous diameter distribution curve of the absorbent hydrogel was obtained (Fig. 13 (b)). A large number of pore structures with pore diameter of 3 to 7 nm were present in the absorbent hydrogel, and the pore diameter of 4.887 nm had the largest content. The content of 25.503 nm was also high between 10 and 50 nm, indicating that the absorbent hydrogel had a very large mesopore content. The pore diameter distribution of the absorbent hydrogel was observed at 50 to 80 nm, and the content of 69.2 nm was the highest, indicating that the absorbent hydrogel contained macropores. The presence of mesoporous and macroporous polymer results in a larger specific surface area and porosity of the absorbent hydrogel.

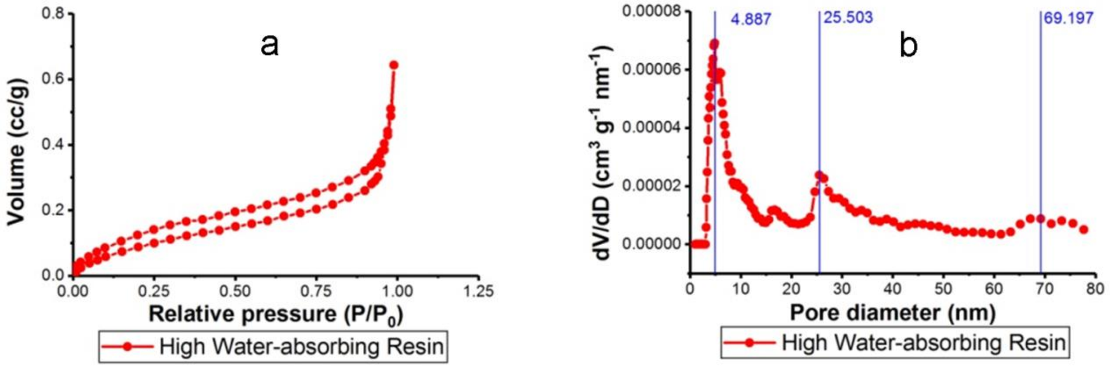

Fig. 13. Nitrogen adsorption-desorption isotherms of micro/nano cellulose and absorbent hydrogel

H-NMR

H-NMR tests were carried out for micro-nano cellulose (Fig. 14 (a)) and absorbent hydrogel (Fig. 14 (b)) to test the grafting of water absorbent groups on micro/nano cellulose. The wide peak at 3 to 4 ppm is the characteristic displacement of 5H on the glucose ring, and the wide peak group between 1.7 and 2.2 ppm corresponds to 3H on the polyacrylic acid CH_2CH. Therefore, it can be seen from the figure that the absorbent groups on the micro-nano cellulose were very well grafted.

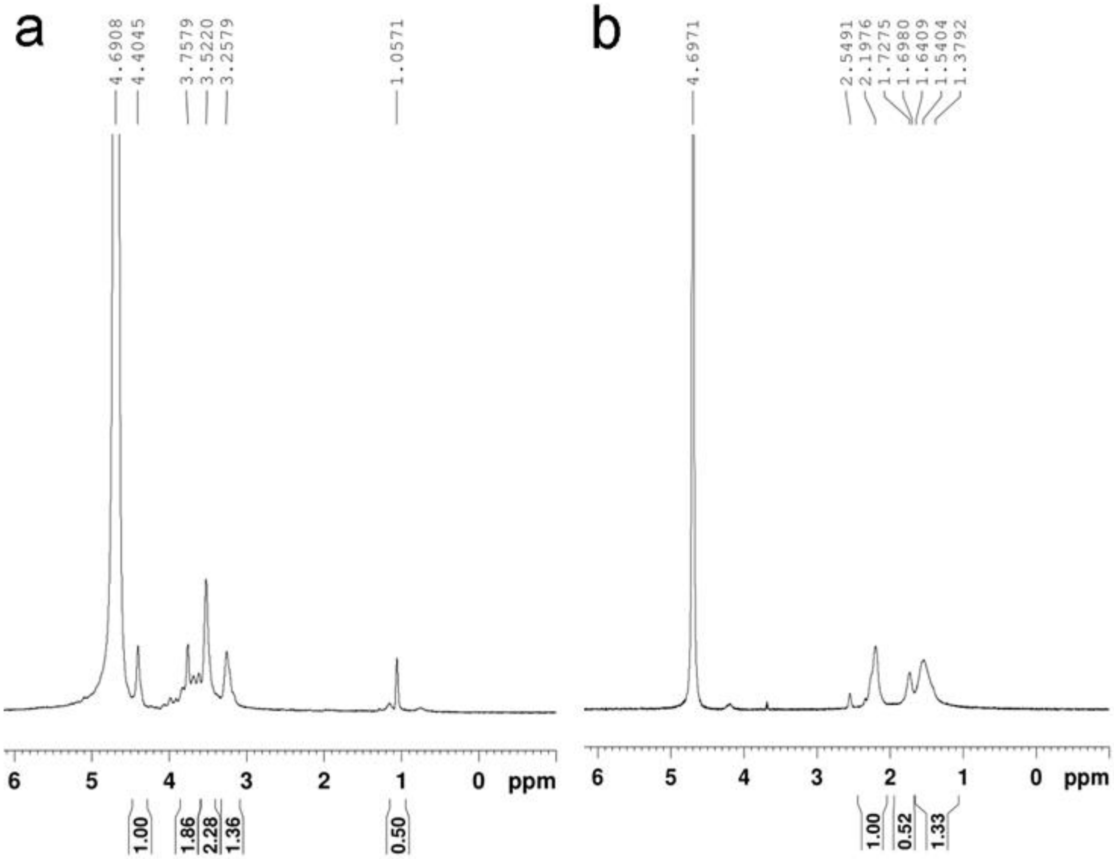

Fig. 14. H-nuclear magnetic resonance spectrum of micro/nano cellulose and absorbent hydrogel

CONCLUSIONS

1. In this work, absorbent hydrogel based on micro/nano cellulose was successfully grafted by two kinds of anionic hydrophilic monomers (AA and AMPS).
2. The influences of reaction factors (micro/nano cellulose mass, initiator APS, cross-linking agent MBA, reaction temperature, AA neutralization, and m(AA):m(AMPS, *etc.*) were investigated concerning the swelling behavior. Results of imbibition curves showed that when conditions were as follows: 11% micro/nano cellulose, 75% neutralized AA, m(AA):m(AMPS) = 7:2, 3% initiator, and 0.3% cross-linking agent at 60 °C, the absorption rate reached the maximum value of 70.16 g/g, 483.91 g/g, and 436.73 g/g in 0.9 wt% sodium chloride solution, 3 wt% urea solution, and rainwater, respectively.

3. The results of FTIR, CLSM, and SEM analyses confirmed that AA and AMPS were grafted onto the surface of micro/nano cellulose. BET results confirmed that the presence of mesoporous and macropores made the absorbent hydrogel highly permeable, allowing the internal and external absorbent groups to absorb water at the same time. H NMR confirmed that the cellulose was grafted with absorbent water groups. The modified absorbent hydrogel will play an important role in the irrigation of agriculture and forestry.

ACKNOWLEDGEMENTS

This work was supported by the Inner Mongolia Technical Plan Project (201802105), the Start-up Project of Inner Mongolia Agricultural University High-level Talents Introduction Scientific Research (NDYB2016-24), and the science research innovation projects of the Inner Mongolia Agricultural University for undergraduates (KJCX2017021).

REFERENCES CITED

Abdelwahab, N. A., Ammar, N. S., and Ibrahim, H. S. (2015). “Graft copolymerization of cellulose acetate for removal and recovery of lead ions from wastewater,” *International Journal of Biological Macromolecules* 79, 913-922. DOI: 10.1016/j.ijbiomac.2015.05.022

Awadallah, F. A., and Mostafa, T. B. (2014). “Synthesis and characterization studies of γ-radiation crosslinked poly(acrylic acid/2-acrylamido-2-methyl propane sulfonic acid) hydrogels,” *Journal of Polymer Engineering* 34(5), 459-469. DOI: 10.1515/polyeng-2013-0067

Chauhan, P., and Yan, N. (2015). “Nanocrystalline cellulose grafted phthalocyanine: A heterogeneous catalyst for selective aerobic oxidation of alcohols and alkyl arenes at room temperature in a green solvent,” *RSC Advances* 5(47), 37517-37520. DOI: 10.1039/c4ra16869k

Chen, J., and Parl, K. (2000). “Synthesis and characterization of superporous hydrogel composites,” *Journal of Controlled Release* 65(1-2), 73-82. DOI: 10.1016/S0168-3659(99)00238-2

Chen, Y. W., Tan, T. H., Lee, H. V., and Abd Hamid, S. B. (2017). “Easy fabrication of highly thermal-stable cellulose nanocrystals using $Cr(NO_3)_3$ catalytic hydrolysis system: A feasibility study from macro- to nano-dimensions,” *Materials* 10(1), Article number 42. DOI: 10.3390/ma10010042

Chen, Z., Liu, M., and Ma, S. (2005). “Synthesis and modification of salt-resistant superabsorbent polymers,” *Reactive and Functional Polymers* 62(1), 85-92. DOI: 10.1016/j.reactfunctpolym.2004.09.003

Choi, J. W., Kim, H. J., Ryu, H., Oh, S., and Choi, S. J. (2019). “Three-dimensional double-network hydrogels of graphene oxide, alginate, and polyacrylonitrile for copper removal from aqueous solution,” *Environmental Engineering Research* 25(6), 924-929. DOI: 10.4491/eer.2019.442

Dai, L., Yang, T., He, J., Deng, L., Liu, J., Wang, L., Lei, J., and Wang, L. (2014). “Cellulose-graft-poly(L-lactic acid) nanoparticles for efficient delivery of anti-cancer drugs," *Journal of Materials Chemistry B* 2(39), 6749-6757. DOI: 10.1039/c4tb00956h

Guo, S. L., and Bu, Y. H. (2013). "Synthesis and application of 2-acrylamido-2-methyl propane sulfonic acid/acrylamide/N, N-dimethyl acrylamide/maleic anhydride as a fluid loss control additive in oil well cementing," *Journal of Applied Polymer Science* 127(5), 3302-3309. DOI: 10.1002/app.37745

Habibi, Y. (2014). "Key advances in the chemical modification of nanocelluloses," *Chemical Society Reviews* 43(5), 1519-1542. DOI: 10.1039/c3cs60204d

He, G., Ke, W., Chen, X., Kong, Y., Zheng, H., Yin, Y., and Cai, W. (2017). "Preparation and properties of quaternary ammonium chitosan-g-poly(acrylic acid-co-acrylamide) superabsorbent hydrogels," *Reactive and Functional Polymers* 111, 14-21. DOI: 10.1016/j.reactfunctpolym.2016.12.001

Hua, S., and Wang, A. (2009). "Synthesis, characterization and swelling behaviors of sodium alginate-g-poly (acrylic acid)/sodium humate superabsorbent," *Carbohydrate Polymers* 75(1), 79-84. DOI: 10.1016/j.carbpol.2008.06.013

Hubbe, M. A., Ayoub, A., Daystar, J. S., Venditti, R. A, and Pawlak, J. J. (2013). "Enhanced absorbent products incorporating cellulose and its derivatives: A review," *BioResources* 8(4), 6556-6629. DOI: 10.15376/biores.8.4.6556-6629

Kabiri, R., and Namazi, H. (2014). "Surface grafting of reduced graphene oxide using nanocrystalline cellulose *via* click reaction," *Journal of Nanoparticle Research* 16, Article number 2474. DOI: 10.1007/s11051-014-2474-3

Klemm, D., Heublein, B., Fink, H. P., and Bohn, A. (2005). "Cellulose: Fascinating biopolymer and sustainable raw material," *Angewandte Chemie International Edition* 44(2), 3358-3393. DOI: 10.1002/anie.200460587

Klinpituksa, P., and Kosaiyakanon, P. (2017), "Superabsorbent polymer based on sodium carboxymethyl cellulose grafted polyacrylic acid by inverse suspension polymerization," *International Journal of Polymer Science* 2017, Article ID 3476921. DOI: 10.1155/2017/3476921

Kosinska, A., Jagielski, J., Ostaszewska, U., Wyszkowska, E., Clozel, M., Kurpaska, L., and Romaniec, M. (2019). "Functional properties of low energy ion-irradiated acrylonitrile-butadiene rubber," *Nuclear Instruments & Methods in Physics Research Section B: Beam Interactions with Materials and Atoms* 443, 15-18. DOI: 10.1016/j.nimb.2018.12.052

Kumar, M., Isloor, A. M., Rao, T. S., Ismail, A. F., Farnwood, R., and Nambissan, P. M. G. (2020). "Removal of toxic arsenic from aqueous media using polyphenylsulfone/ cellulose acetate hollow fiber membranes containing zirconium oxide," *Chemical Engineering Journal* 393, Article ID 124367. DOI: 10.1016/j.cej.2020.124367

Lan, G., Zhang, M., Liu, Y., Qiu, H., Xue, S., Zhang, T., and Xu, Q. (2019). "Synthesis and swelling behavior of super-absorbent soluble starch-*g*-poly(AM-*co*-NaAMC$_{14}$S) through graft copolymerization and hydrolysis," *Starch* 71(5-6), Article ID 1800272. DOI: 10.1002/star.201800272

Liu, C. Y., Zhang, M. J., Zhu, J., and Ma, S. S. (2008). "Synthesis and characterization of a salt-resisting superabsorbent based on poly(acrylic acid) with sodium tungstate as a crosslinker," *Journal of Applied Polymer Science* 110(4), 2440-2445. DOI: 10.1002/app.28258

Liu, C., Lei, F., Li, P., Jiang, J., and Wang, K. (2020). "Borax crosslinked fenugreek galactomannan hydrogel as potential water-retaining agent in agriculture," *Carbohydrate Polymers* 236, Article ID 116100. DOI: 10.1016/j.carbpol.2020.116100

Liu, Z., Miao, Y., Wang, Z., and Yin, G. (2009). "Synthesis and characterization of a novel super-absorbent based on chemically modified pulverized wheat straw and acrylic acid," *Carbohydrate Polymers* 77(1), 131-135. DOI: 10.1016/j.carbpol.2008.12.019

Lu, Q., Cai, Z., Wang, S., Lin, F., Lu, B., Chen, Y., and Huang, B. (2017). "Controlled construction of nanostructured organic-inorganic hybrid material induced by nanocellulose," *ACS Sustainable Chemistry & Engineering* 5(9), 8456-8463. DOI: 10.1021/acssuschemeng.7b02394

Madrid, J. F., and Abad, L. V. (2015). "Modification of microcrystalline cellulose by gamma radiation-induced grafting," *Radiation Physics and Chemistry* 115, 143-147. DOI: 10.1016/j.radphyschem.2015.06.025

Mandal, A., and Chakrabarty, D. (2017). "Synthesis and characterization of nanocellulose reinforced full-interpenetrating polymer network based on poly(vinyl alcohol) and polyacrylamide (both crosslinked) composite films," *Polymer Composites* 38(8), 1720-1731. DOI: 10.1002/pc.23742

Miao, Z. C., Wang, F., Deng, D., Zhang, Y. M., Wang, L., and Li, Z. J. (2012). "Preparation of cellulose-graft superabsorbent hydrogel," *Advanced Materials Research* 557-559, 1018-1021. DOI: 10.4028/www.scientific.net/AMR.557-559.1018

Mohammadkazemi, F., Doosthoseini, K., Ganjian, E., and Azin, M. (2015). "Manufacturing of bacterial nano-cellulose reinforced fiber-cement composites," *Construction and Building Materials* 101(Part 1), 958-964. DOI: 10.1016/j.conbuildmat.2015.10.093

Qiao, D., Liu, H., Yu, L., Bao, X., Simon, G. P., Petinakis, E., and Chen, L. (2016). "Preparation and characterization of slow-release fertilizer encapsulated by starch-based superabsorbent polymer," *Carbohydrate Polymers* 147, 146-154. DOI: 10.1016/j.carbpol.2016.04.010

Quennouz, N., Hashmi, S. M., Choi, H. S., Kim, J. W., and Osuji, C. O. (2016). "Rheology of cellulose nanofibrils in the presence of surfactants," *Soft Matter* 12(1), 157-164. DOI: 10.1039/c5sm01803j

Rahman, M. L., Sarkar, S. M., Yusoff, M. M., and Abdullah, M. H. (2016). "Efficient removal of transition metal ions using poly(amidoxime) ligand from polymer grafted kenaf cellulose," *RSC Advances* 6(1), 745-757. DOI: 10.1039/c5ra18502e

Saikia, A. K., Aggarwal, S., and Mandal, U. K. (2012). "Swelling dynamics of poly(NIPAM-co-AMPS) hydrogels synthesized using PEG as macroinitiator: Effect of AMPS content," *Journal of Polymer Research* 20, Article number 31. DOI: 10.1007/s10965-012-0031-2

Song, X. F., and He, T. S. (2012). "Resistance to carbonation of concrete treated by superabsorbent hydrogel synthesized *in situ*," *Advanced Materials Research* 374-377, 1872-1876. DOI: 10.4028/www.scientific.net/AMR.374-377.1872

Varaprasad, K., Jayaramudu, T., and Sadiku, E. R. (2017). "Removal of dye by carboxymethyl cellulose, acrylamide and graphene oxide *via* a free radical polymerization process," *Carbohydrate Polymers* 164, 186-194. DOI: 10.1016/j.carbpol.2017.01.094

Wang, J., Wang, W., and Wang, A. (2010). "Synthesis, characterization and swelling behaviors of hydroxyethyl cellulose-g-poly(acrylic acid)/attapulgite superabsorbent composite," *Polymer Engineering & Science* 50(5), 1019-1027. DOI: 10.1002/pen.21500

Wen, Y., Wei, B., Cheng, D., An, X., and Ni, Y. (2017). "Stability enhancement of nanofibrillated cellulose in electrolytes through grafting of 2-acrylamido-2-methylpropane sulfonic acid," *Cellulose* 24, 731-738. DOI: 10.1007/s10570-016-1182-9

Wu, B., Ma, Z., and Yan, N. (2020). "Agricultural drought mitigating indices derived from the changes in drought characteristics," *Remote Sensing of Environment* 244, Article ID 111813. DOI: 10.1016/j.rse.2020.111813

Wu, F., Zhang, Y., Liu, L., and Yao, J. (2012). "Synthesis and characterization of a novel cellulose-g-poly(acrylic acid-co-acrylamide) superabsorbent composite based on flaxyarn waste," *Carbohydrate Polymers* 87(4), 2519-2525. DOI: 10.1016/j.carbpol.2011.11.028

Wu, L., and Liu, M. (2007). "Slow-release potassium silicate fertilizer with the function of superabsorbent and water retention," *Industrial & Engineering Chemistry Research* 46(20), 6494-6500. DOI: 10.1021/ie070573l

Yang, J., Lu, S., Pan, L., Luo, Q., Song, L., Wu, L., and Yu, J. (2017). "Effect of epoxidized soybean oil grafted poly (12-hydroxy stearate) on mechanical and thermal properties of microcrystalline cellulose fibers/polypropylene composites," *Polymer Bulletin* 74, 911-930. DOI: 10.1007/s00289-016-1753-9

Zaman, M., Liu, H., Xiao, H., Chibante, F., and Ni, Y. (2013). "Hydrophilic modification of polyester fabric by applying nanocrystalline cellulose containing surface finish," *Carbohydrate Polymers* 91(2), 560-567. DOI: 10.1016/j.carbpol.2012.08.070

Article submitted: June 25, 2020; Peer review completed: September 12, 2020; Revised version received and accepted: December 11, 2020; Published: December 22, 2020.
DOI: 10.15376/biores.16.1.1256-1275